Universität Rostock Traditio et Innovatio

Impact of stellar variability on the observational appearance of protoplanetary disks

Alexandra Botnariuc

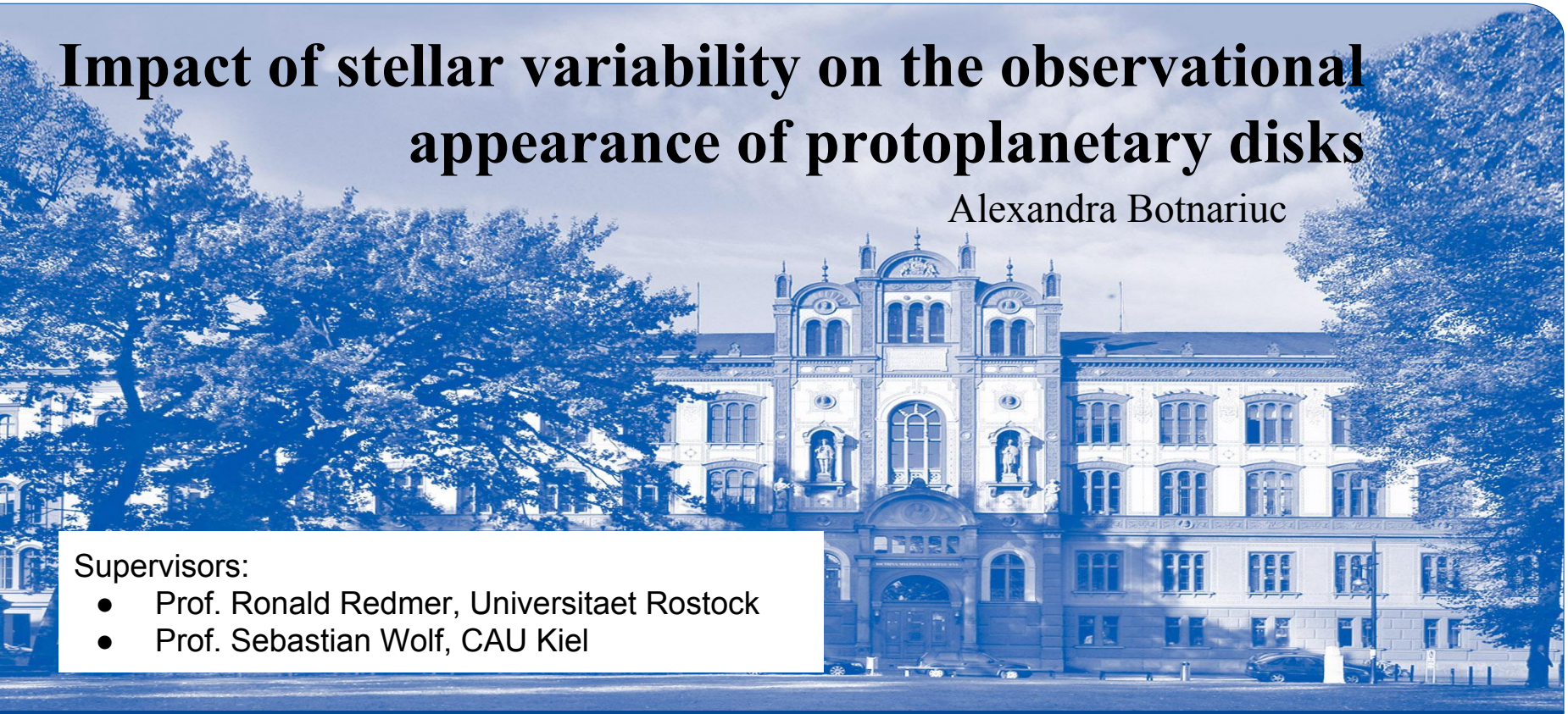

Supervisors:

- Prof. Ronald Redmer, Universitaet Rostock
- Prof. Sebastian Wolf, CAU Kiel

Overview

1. Introduction and motivation
2. Observations and instruments
3. Visibility curves
4. Method
5. Results
6. Conclusions

T Tauri Stars

Spectral type	late K, F, G or early M
T_{eff}	$3500 - 9000\,\mathrm{K}$
$M_\star$	$1 - 3\,\mathrm{M}_\odot$
$R_\star$	$2 - 6\,\mathrm{R}_\odot$
$L_\star$	$0.1 - 50\,\mathrm{L}_\odot$

$$L = 4\pi R^2 \sigma T_{\mathrm{eff}}^4$$

$$\frac{L}{L_\odot} = \left(\frac{T}{T_\odot}\right)^4 \left(\frac{R}{R_\odot}\right)^2$$

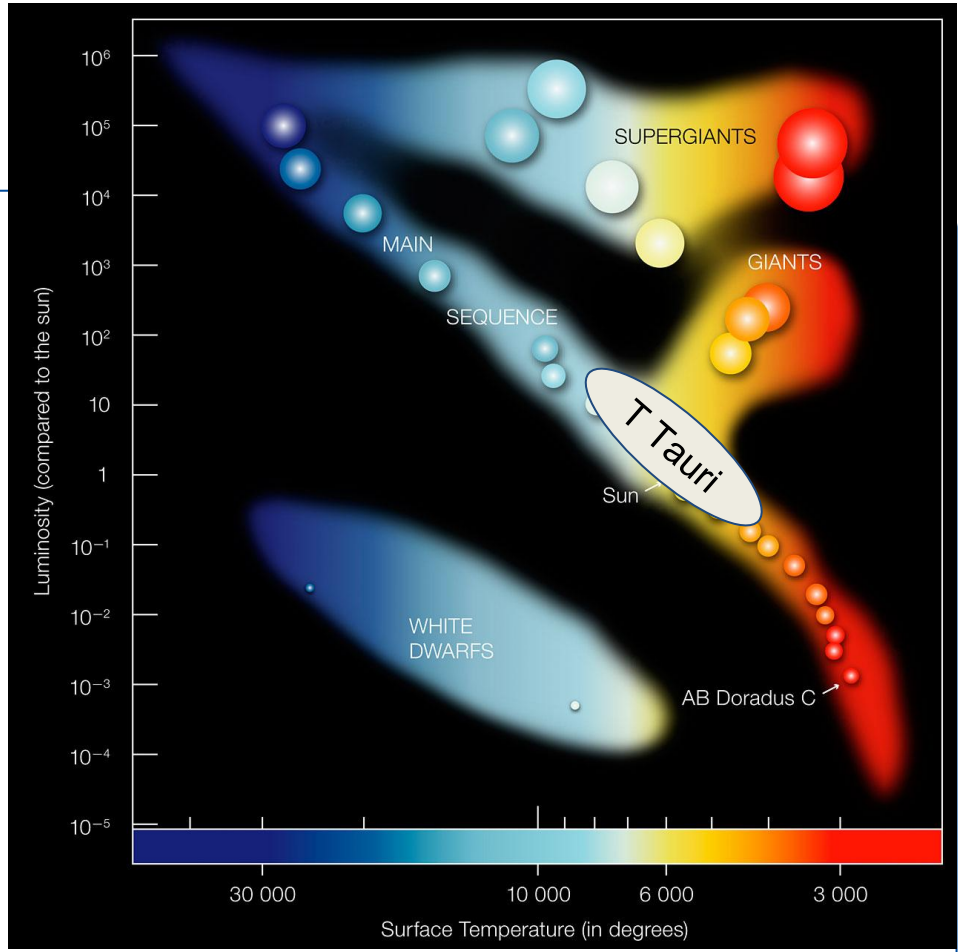

Figure 1: Hertzsprung-Russell Diagram **Credit:** ESO

Luminosity variability

Figure 2: Herbig-Haro object **(HH) 212**, located in Horsehead Nebula star-forming region.

Credit: ESO/M. McCaughrean

$$m_x = -2.5 \log_{10} \left(\frac{F_x}{F_{x,0}} \right)$$

The curious case of DR Tau

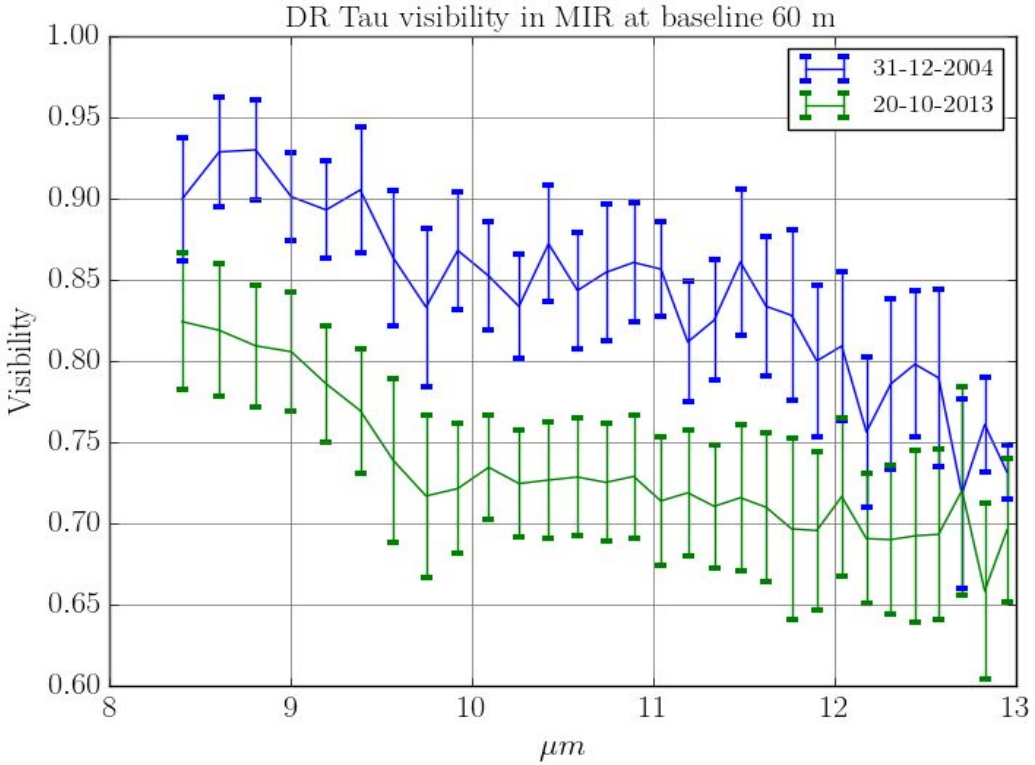

	DR Tau Parameters
$T_\star$	4050 K
$L_\star$	$0.9 - 15\,\mathrm{L}_\odot$
T_{accr}	8000 K
L_{accr}	$1\,\mathrm{L}_\odot$
R_{in}	0.065 AU
R_{ou}	350 AU
β	1.025
h_0	10.0 AU
M_{disk}	$3 \cdot 10^{-3}\mathrm{M}_\odot$

Model B, R. Brunngräber, 2018

Circumstellar disks

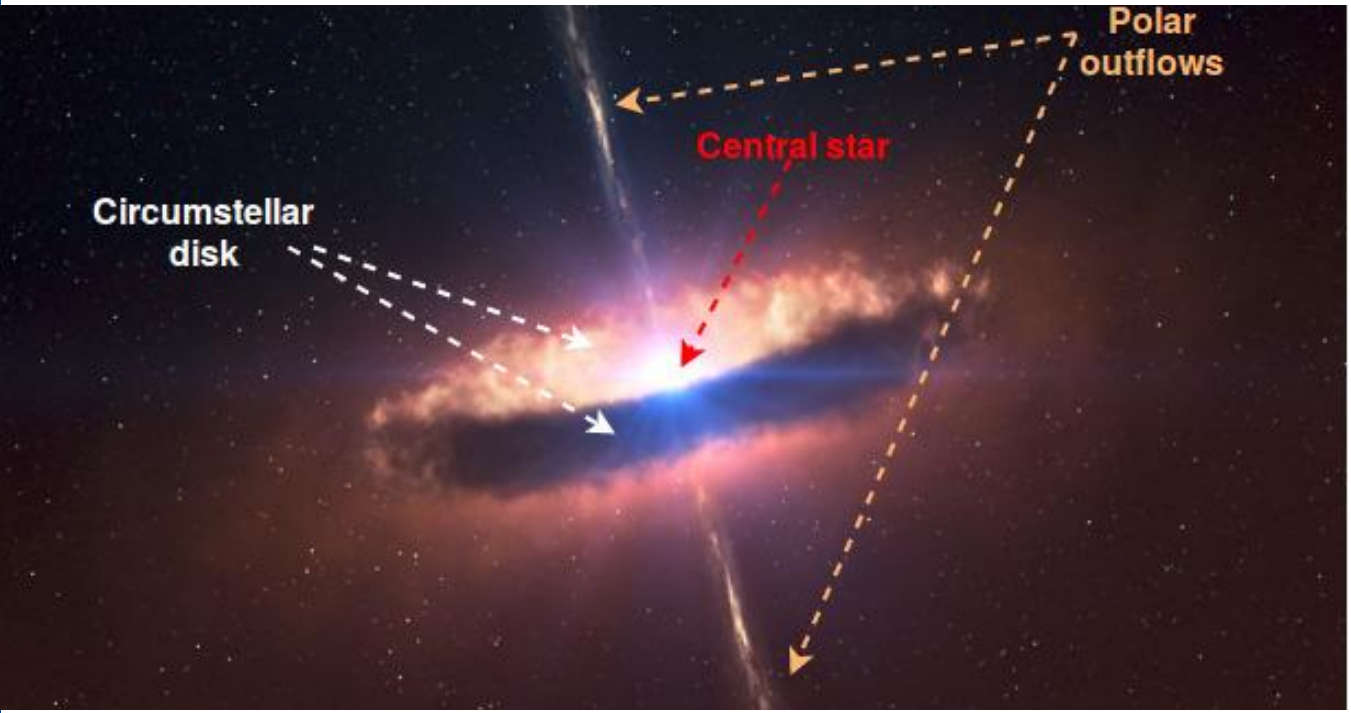

Figure 3: Circumstellar disk **Credit:** ESO/L. Calçada/M. Kornmesser

Figure 4: V883 Orionis [ALMA in long-baseline mode].

Credit:ALMA (ESO/NAOJ/NRAO)/L. Cieza

Circumstellar disks

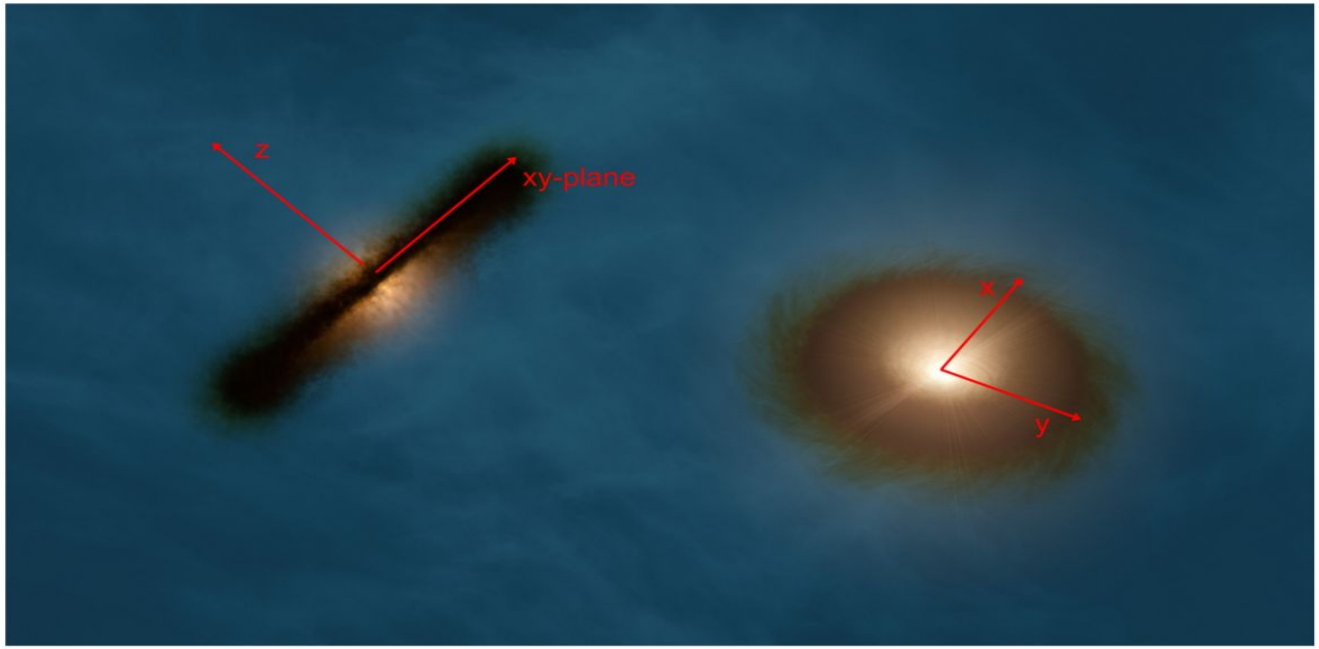

(a) Artist impression of two circumstellar disks. The one on the left is seen edge on by the observer, while the disk on the right is almost face-on with a slight incline towards the observer. Cartesians coordinates as used in this thesis are added in red.

Credit: ESO

Protoplanetary disk model [5]

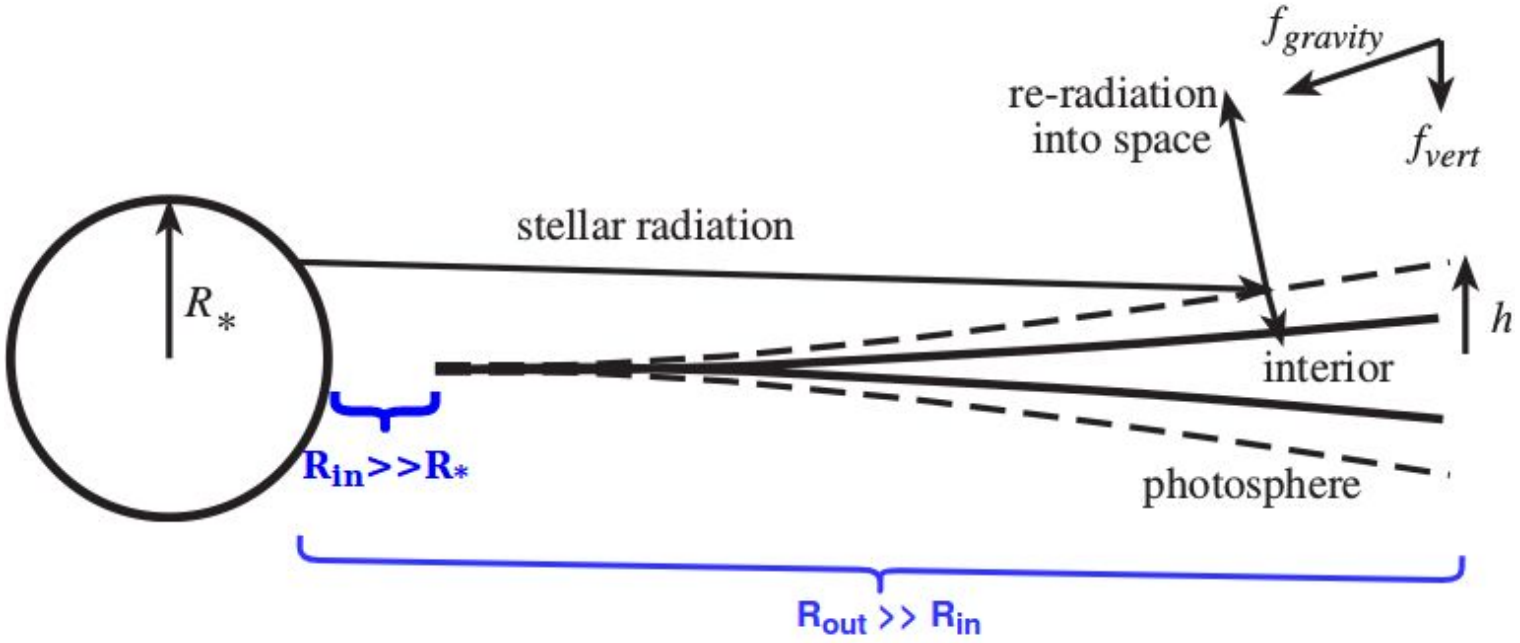

Figure 5: Flaring disk in xz plane. **Credit:** Beckwith, 1999 (adaptation in blue)

Disk density distribution

$$\rho(r,z)^{\mathrm{Sh-Su}} = \left(\frac{r}{100}\right)^{-\alpha} \exp\left(-\frac{1}{2}\frac{z^2}{h(r)^2}\right),$$

$$h(r) = h_0 \left(\frac{r}{100}\right)^{\beta}, \alpha = 2.625, \beta = 1.125, h_0 = 10\mathrm{AU}$$

$$\rho(r,z)^{\mathrm{Ly-P}} = \rho(r,z)^{\mathrm{Sh-Su}} \exp\left(\left(-\frac{r}{100}\right)^{(2+\beta-\alpha)}\right)$$

Disk parameters:

M_{disk}	$10^{-5} - 10^{-7}\,\mathrm{M}_{\odot}$
R_{in}	$0.07 - 10\,\mathrm{AU}$
R_{out}	$100 - 300\,\mathrm{AU}$

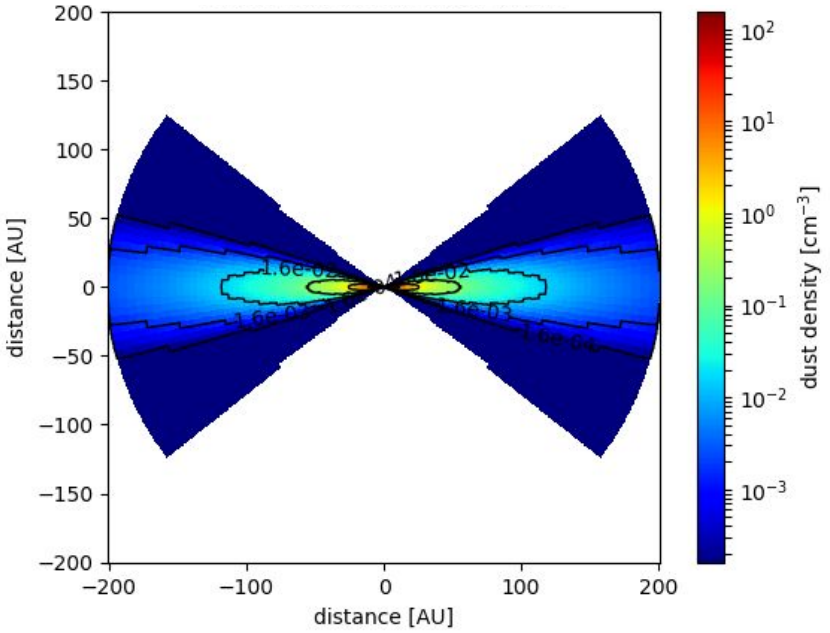

Figure 6: Dust number density in *xz*-plane

$L = 1.5L_{\odot}$, $T = 6000\mathrm{K}$, $\mathrm{R_{in}} = 1\mathrm{AU}$

Figure 7: Temperature in *xz*-plane

$L = 1.5L_{\odot}$, $T = 6000\mathrm{K}$, $\mathrm{R_{in}} = 1\mathrm{AU}$

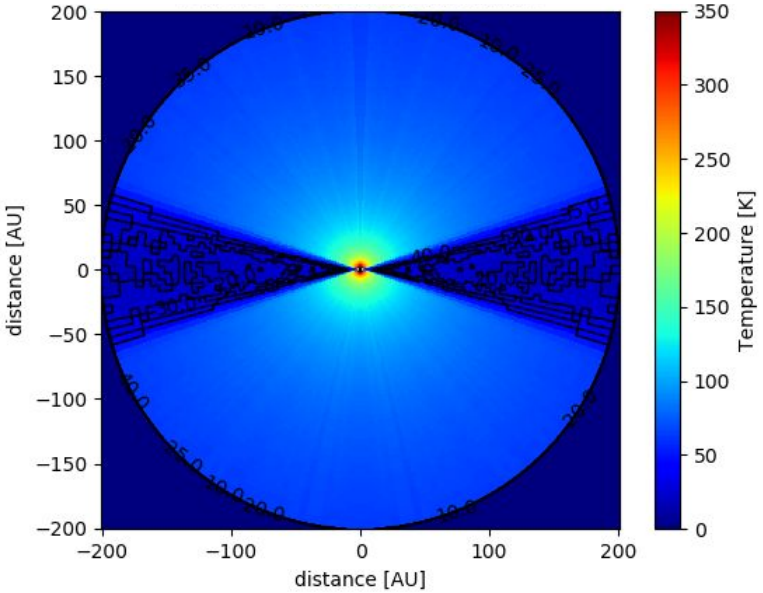

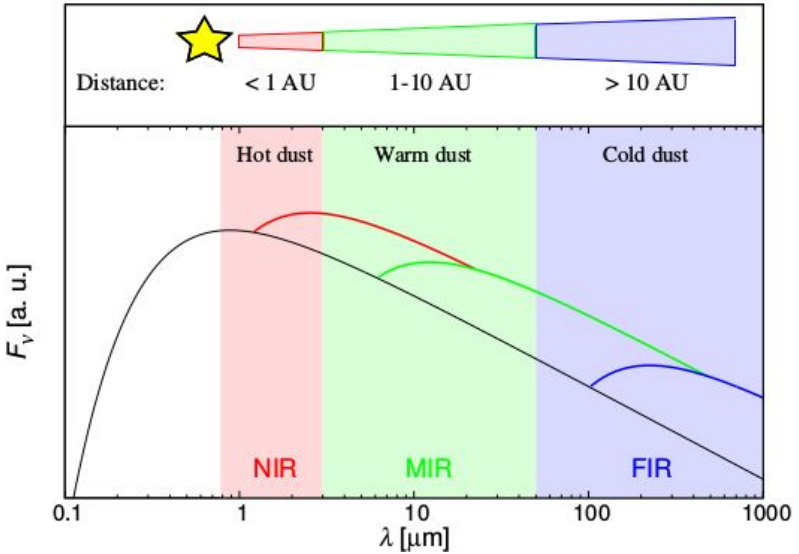

Figure 8: Illustration of inner edge dust contributions to different parts of the SED. The dark line corresponds to a sun-like star, and the flux maxima are arbitrary. **Credit:** Kirchschlager et al., 2017

2. How do we observe circumstellar disks?

VLTI

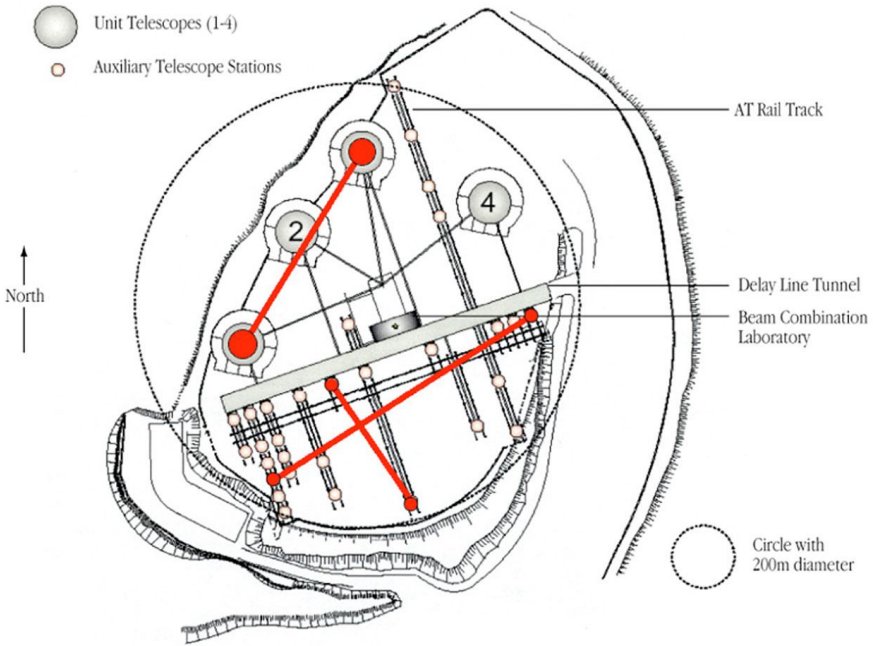

Figure 9: Schematic of VLT array
Credit: ESO

Figure 10: The Unit telescopes at VLT, Paranal Observatory, Atacama Desert, Chile, 2 635 m
Credit: ESO

Visibility

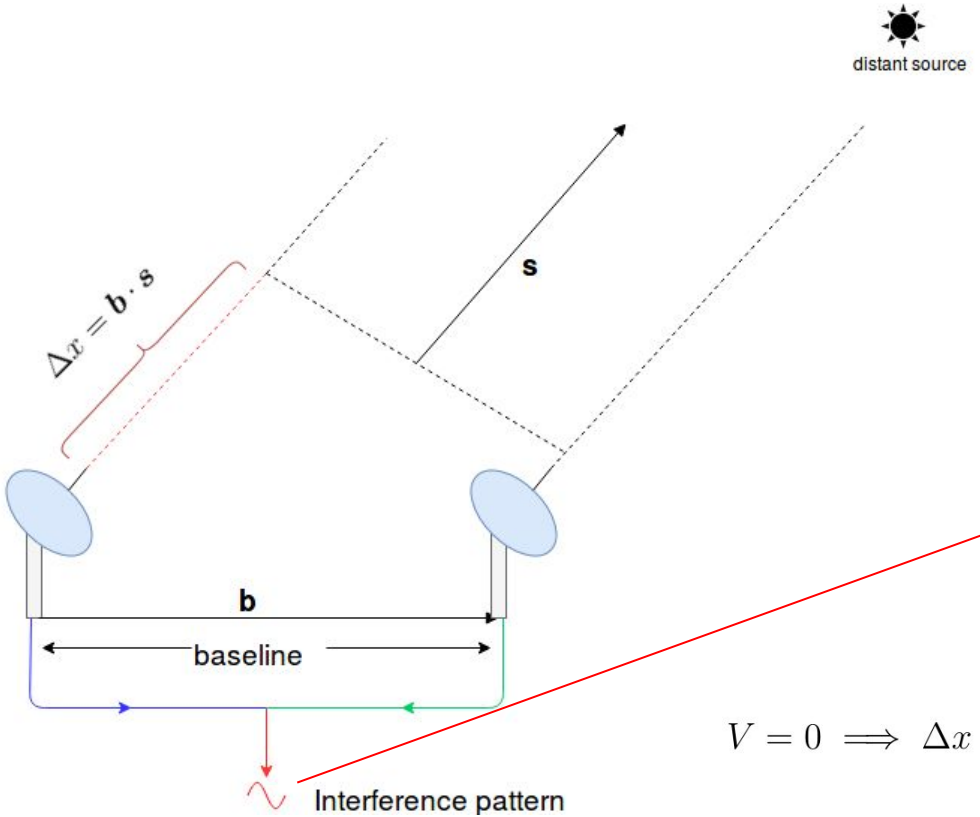

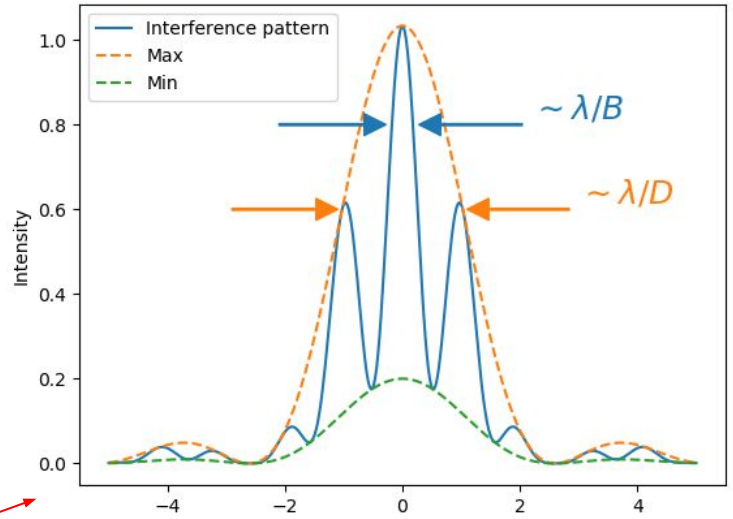

$$V = \frac{I_{\max} - I_{\min}}{I_{\max} + I_{\min}} \qquad V = \frac{2\sqrt{I_1 I_2}}{I_1 + I_2}$$

$$V = 0 \implies \Delta x = b \cdot s \cdot \theta = (2k+1)\lambda \implies b = \frac{(2k+1)\lambda}{s\theta}$$

Visibility

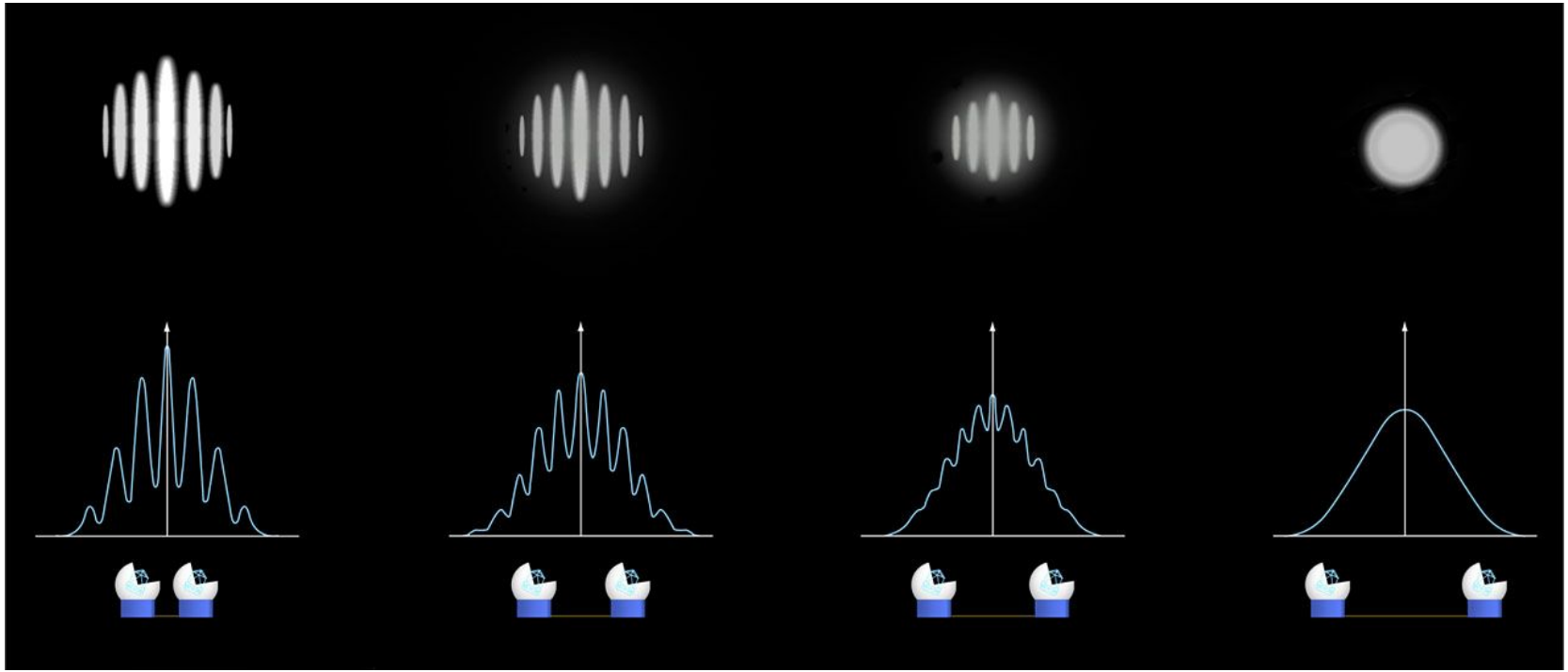

Interference fringes in relation to telescope baseline.

Credit: ESO

Visibility μ

The Van-Cittert / Zernike theorem: the complex visibility μ, for a non-coherent and almost monochromatic extended source is the normalized Fourier Transform ($\mathcal{FT}$) of the brightness distribution ($I(x,y)$):

$$\mu(\boldsymbol{b},\lambda) = \frac{\mathcal{FT}(I(x,y))}{\oiint I(x,y)}$$

$$\mu(u,v) = \frac{\iint_{-\infty}^{\infty} I(x,y)e^{2\pi i(ux+vy)}\,\mathrm{d}x\,\mathrm{d}y}{\iint_{-\infty}^{\infty} I(x,y)\,\mathrm{d}x\,\mathrm{d}y}, \text{ where } \mathrm{u} = \frac{\mathrm{b_x}}{\lambda}, \mathrm{v} = \frac{\mathrm{b_y}}{\lambda}$$

$$V(u,v) = \|\mu(u,v)\| \in [0,1]$$

Visibility V

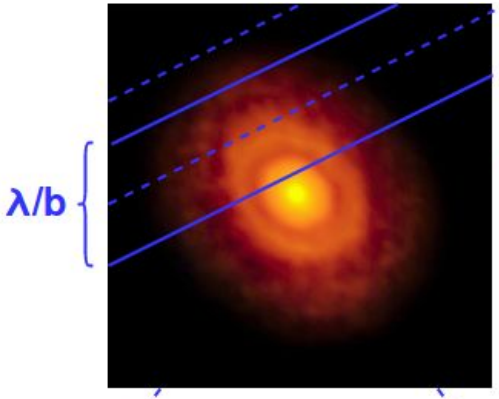

$$\theta_{\text{res}} \propto \frac{\lambda}{D}$$

Inverse Fourier Transform

Repeat over all possible baselines

b

baseline

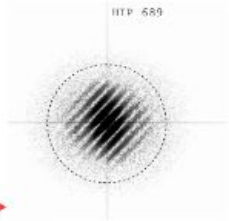

Interference pattern

Visibility V

Visibility V, s = 140 pc

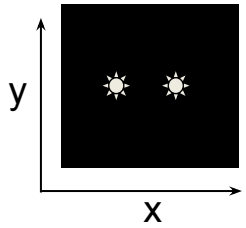

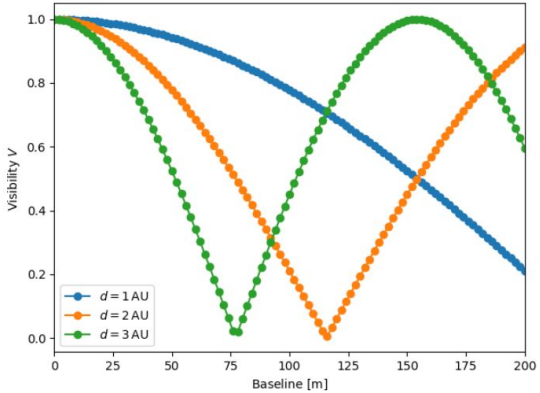

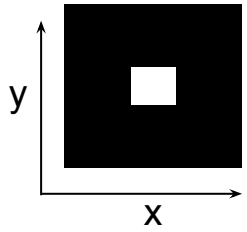

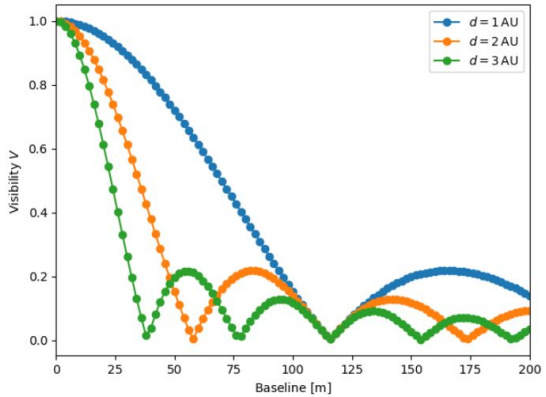

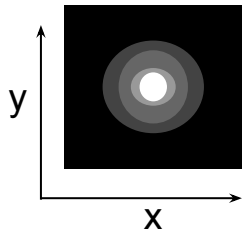

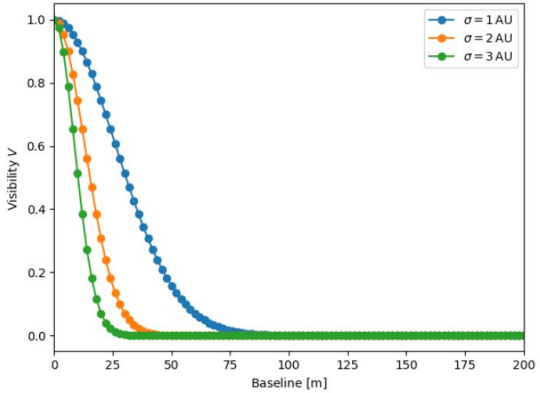

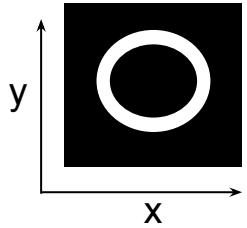

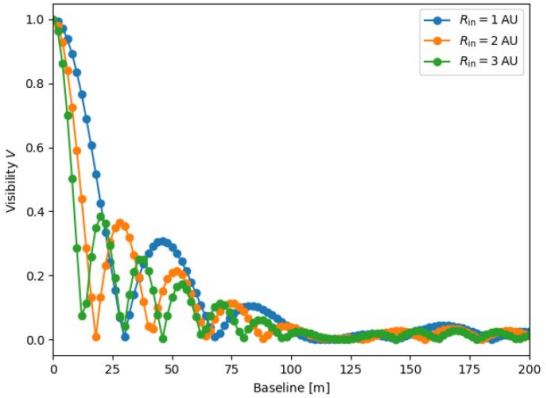

Method

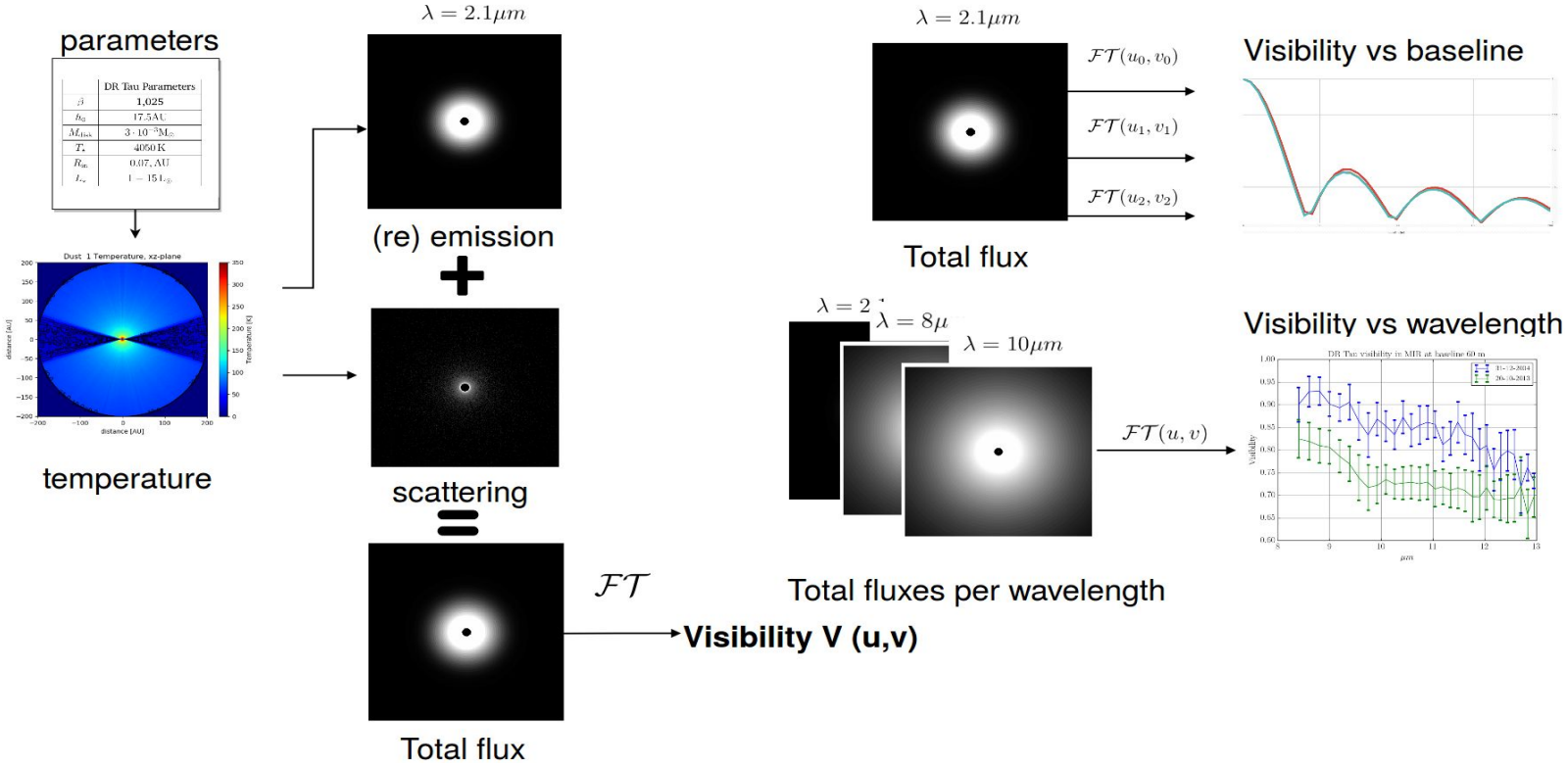
parameters
DR Tau Parameters
1,025
17.5AU
$3 \cdot 10^{-3}M_{\odot}$
4050 K
0.07, AU
$1 - 15 l_{\odot}$
Dust 1 Temperature, xz-plane
distance [AU]
Temperature [K]
temperature
$\lambda = 2.1\mu m$
(re) emission
scattering
Total flux
$\mathcal{FT}$
Visibility V (u,v)
$\lambda = 2.1\mu m$
$\mathcal{FT}(u_0, v_0)$
$\mathcal{FT}(u_1, v_1)$
$\mathcal{FT}(u_2, v_2)$
Total flux
Visibility vs baseline
$\lambda = 8\mu$
$\lambda = 10\mu m$
$\mathcal{FT}(u, v)$
Total fluxes per wavelength
Visibility vs wavelength
DR Tau visibility in MIR at baseline 60 m
Visibility
μm

Quick result analysis

$$b^{\min} = \frac{\lambda}{s\theta}$$

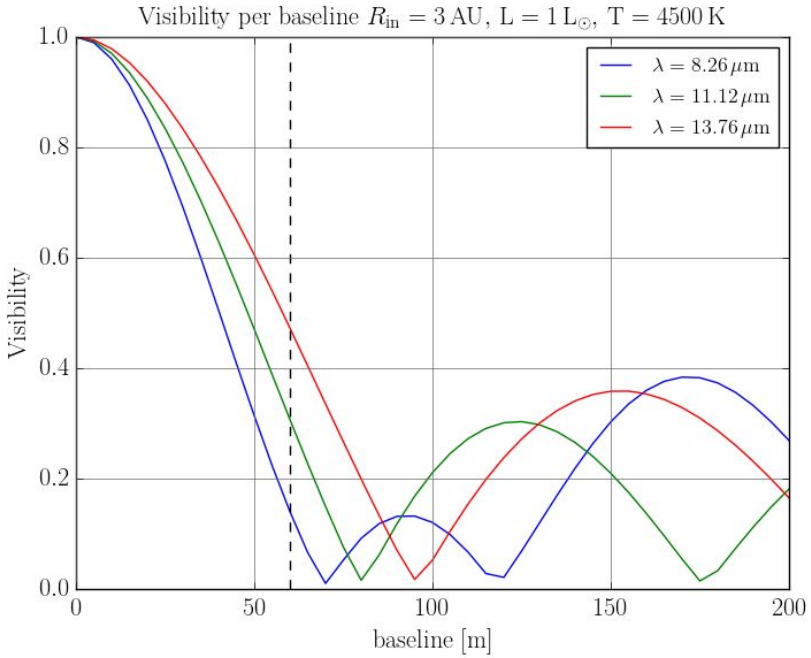

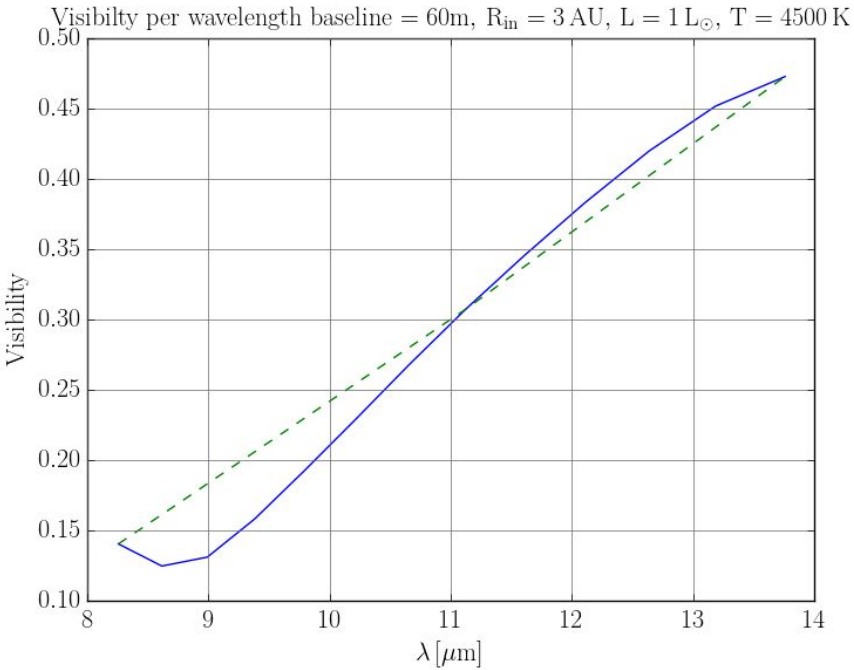

Temperature and inner radius variation

$$b^{\min} = \frac{\lambda}{s\theta}$$

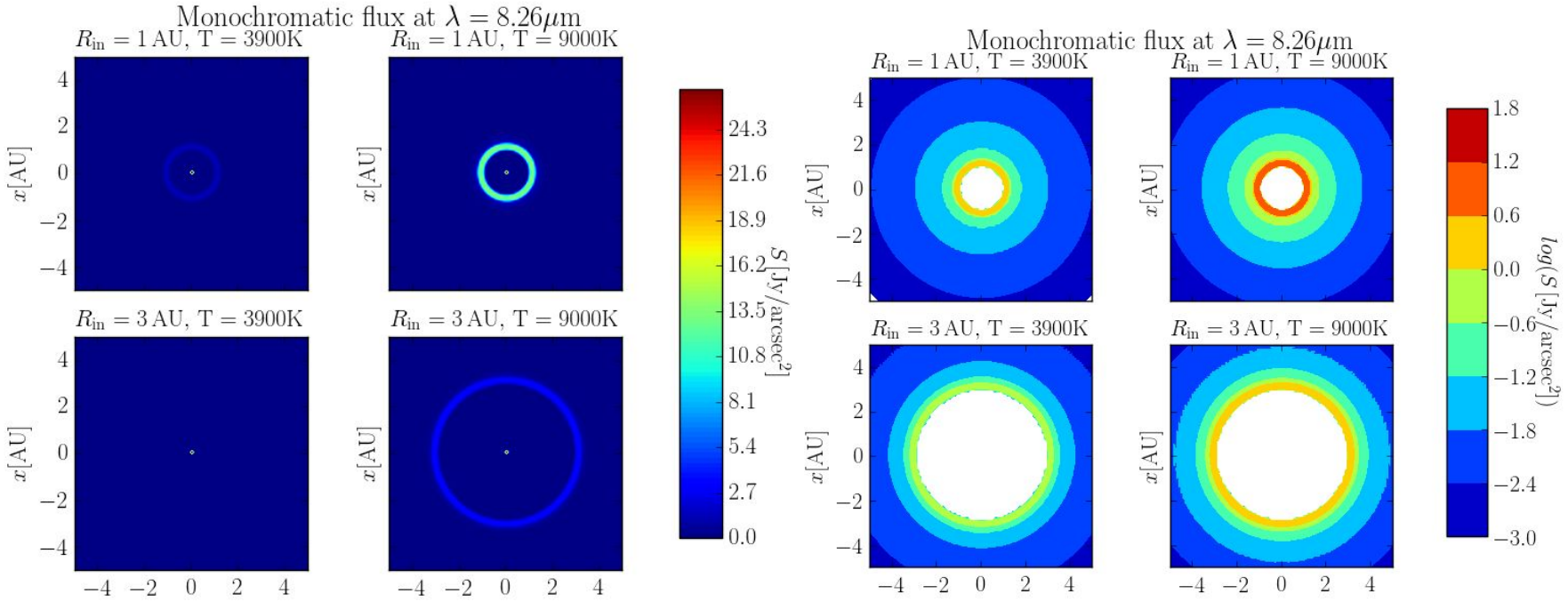

Temperature and inner radius variation

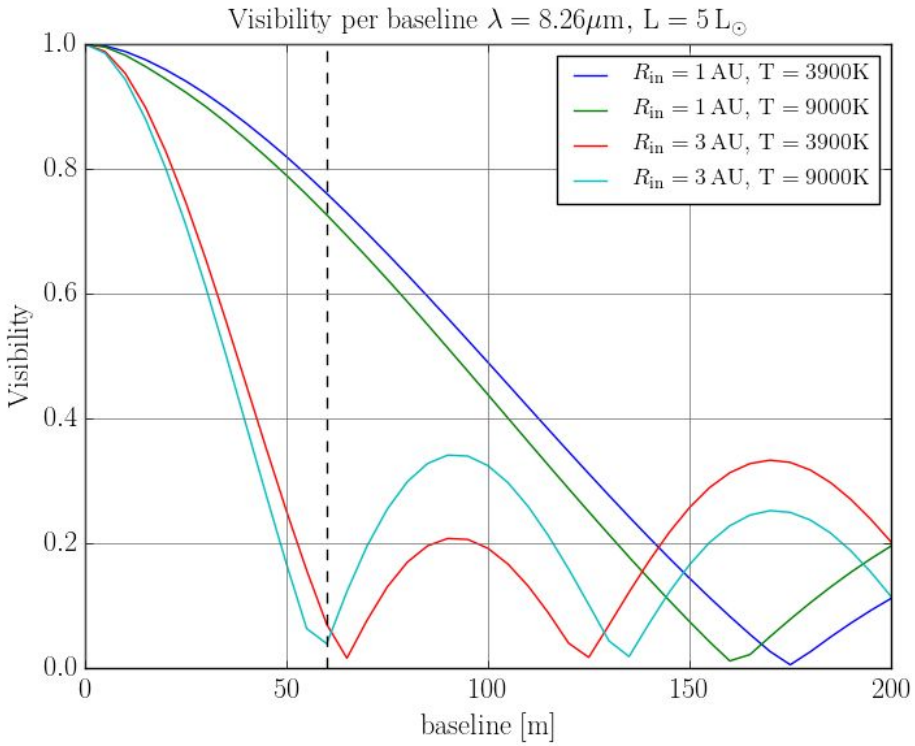

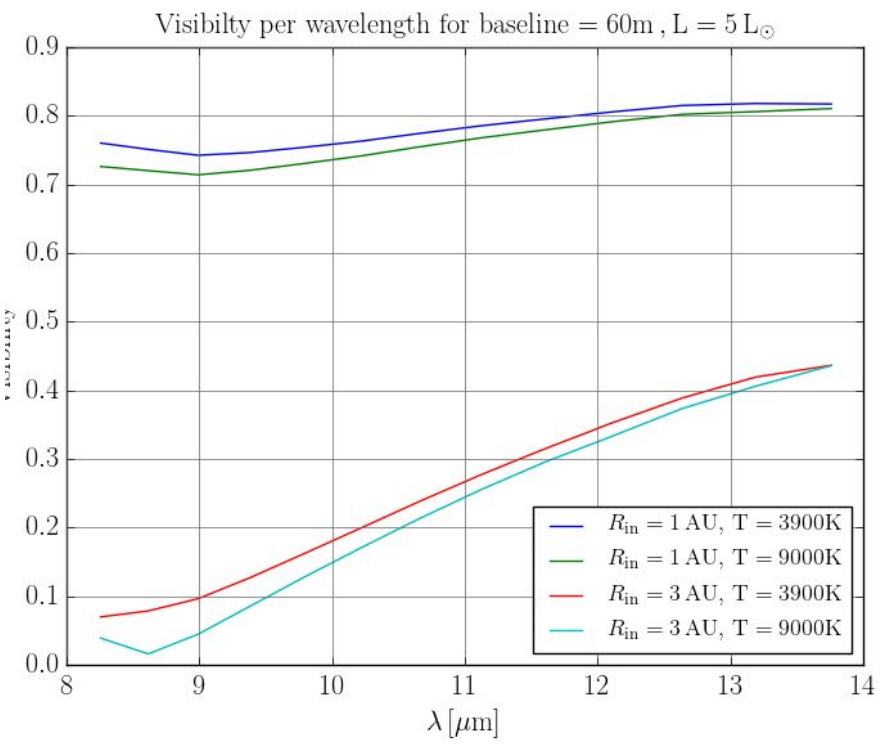

Luminosity variation

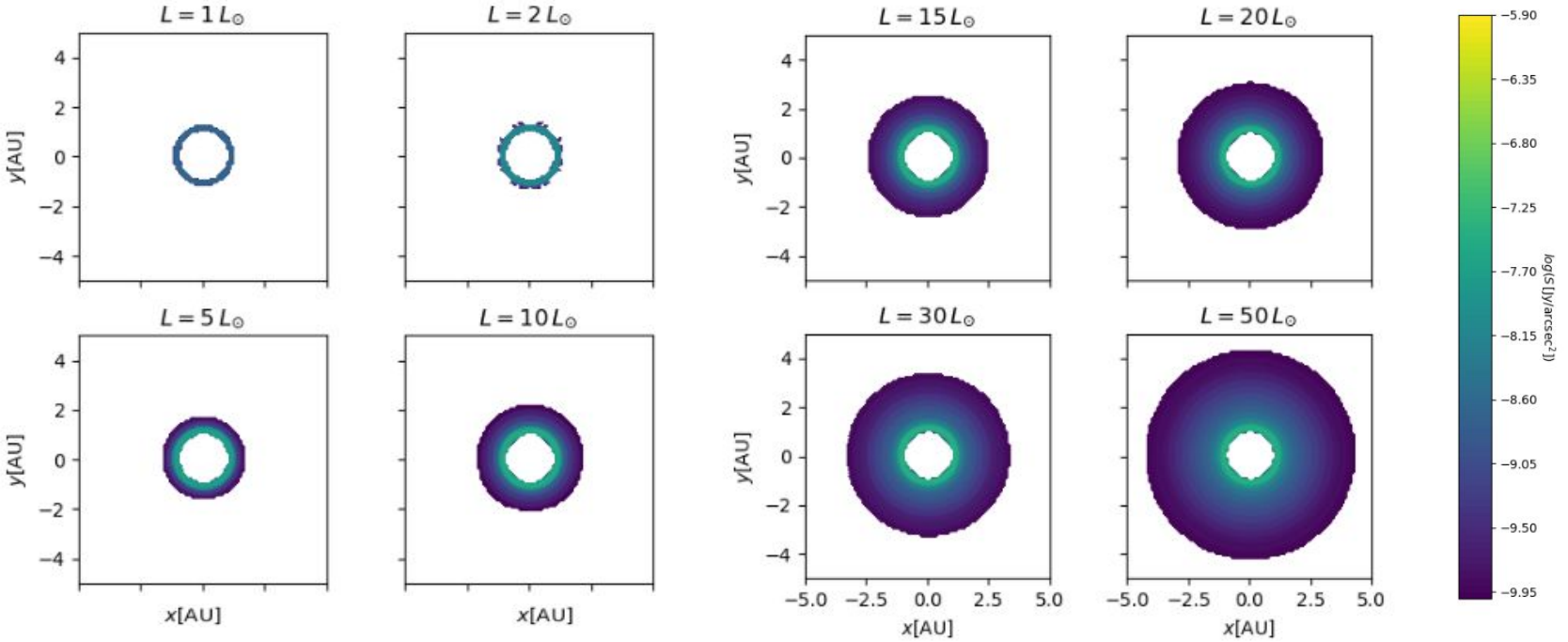

Variation of brightness with luminosity at λ = 8.2 μm, for a disk with R_{in} = 1 AU, and star with $T_\star$ = 3900 K, cut-off value at $5 \cdot 10^{-11}$ Jy/arcsec^2

Luminosity variation MIR

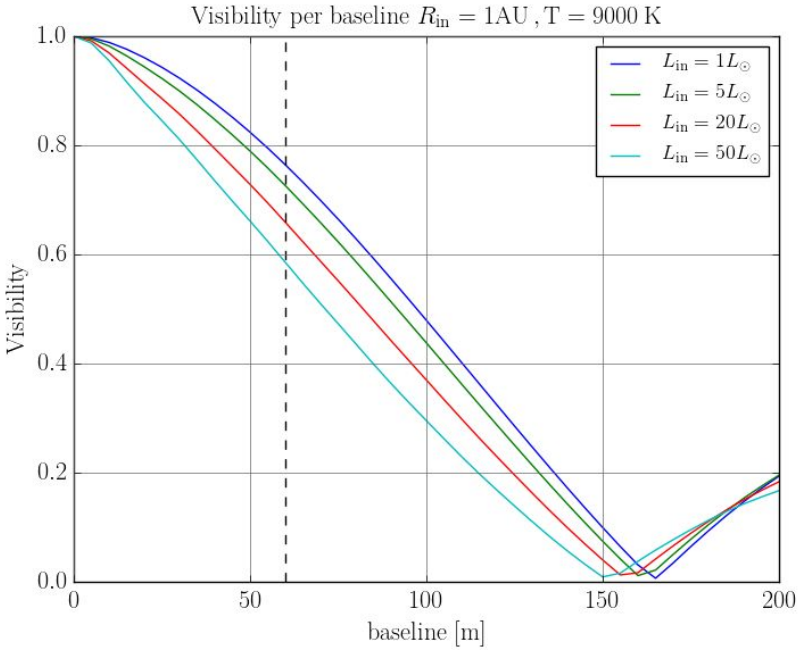

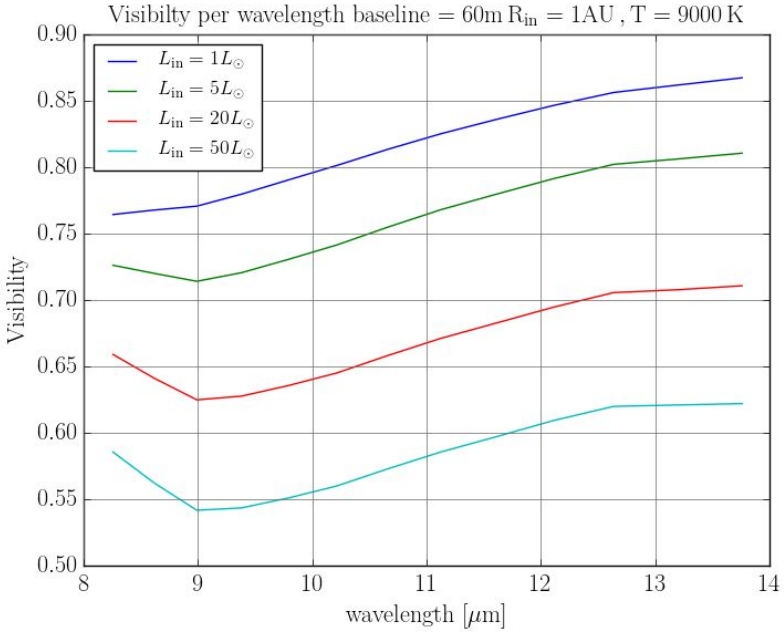

Luminosity variation MIR

		$R_{\text{in}} = 0.1\,\text{AU}$	$R_{\text{in}} = 1\,\text{AU}$	$R_{\text{in}} = 2\,\text{AU}$	$R_{\text{in}} = 3\,\text{AU}$
$T = 3900\,\text{K}$	**avg**	0.415	0.268	0.189	0.154
	max	0.467	0.327	0.226	0.216
$T = 4500\,\text{K}$	**avg**	0.431	0.274	0.186	0.144
	max	0.469	0.324	0.222	0.166
$T = 5000\,\text{K}$	**avg**	0.436	0.268	0.179	0.147
	max	0.481	0.320	0.222	0.165
$T = 7000\,\text{K}$	**avg**	0.445	0.272	0.179	0.129
	max	0.466	0.327	0.221	0.160
$T = 9000\,\text{K}$	**avg**	0.437	0.271	0.167	0.118
	max	0.469	0.325	0.211	0.150

Table 3.4.: Visibility variation over the MIR (avg=average and **max**=maximum) for baselines in $[0, 200]\,\text{m}$ for different temperatures and inner radii

Luminosity variation NIR

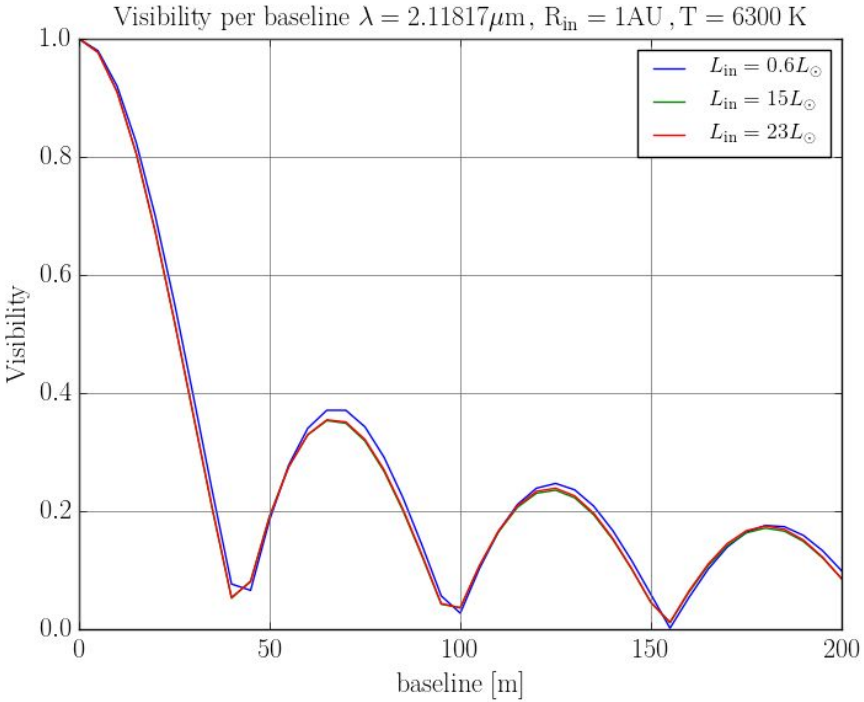

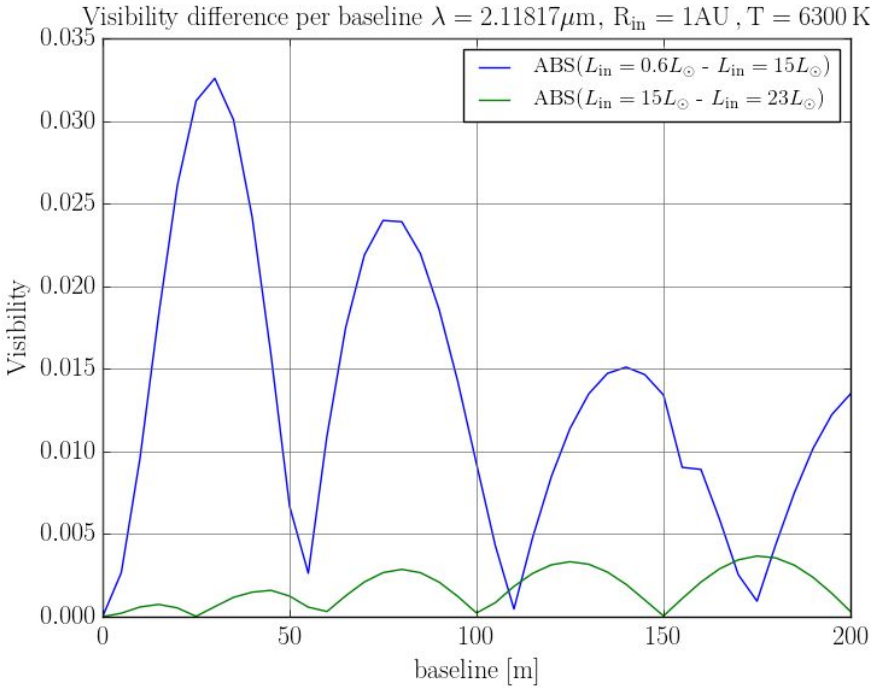

DR Tau: visibility against wavelength

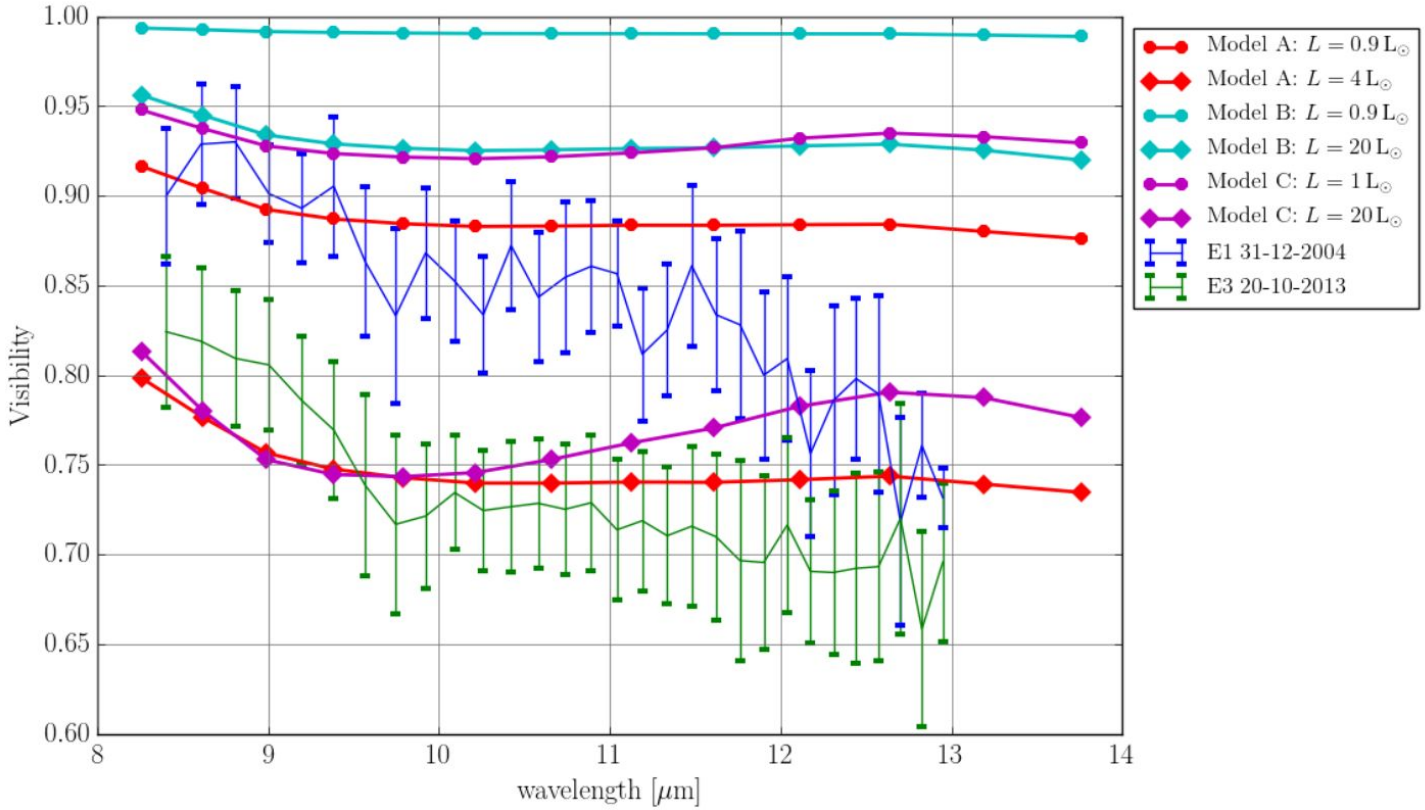

Conclusions

- in the parameter space explored [1 − 50L_*], greatest influence in the MIR
- little to no consequence in the NIR (maximum variance 3.82%)
- maximum variance caused by a change in luminosity is of **48.1%** (T = 5 000 K, R_{in} = 0.1 AU at λ = 13.76 μm, L=50L_0)
- Knowing the inner radius and the geometry of the disk, one could, with sufficient simulations determine the relation between the drop in visibility and the increase in luminosity
- A change in magnitude of 1.6 is sufficient to account for a similar drop in visibility to the data on DR Tau
- DR Tau is not fitted by current models, and there are other possible causes for the change in visibility (porosity of grains, change in radius of disk, geometry etc)

Thank you!

Questions?

Extra Slides

A1. Star Formation

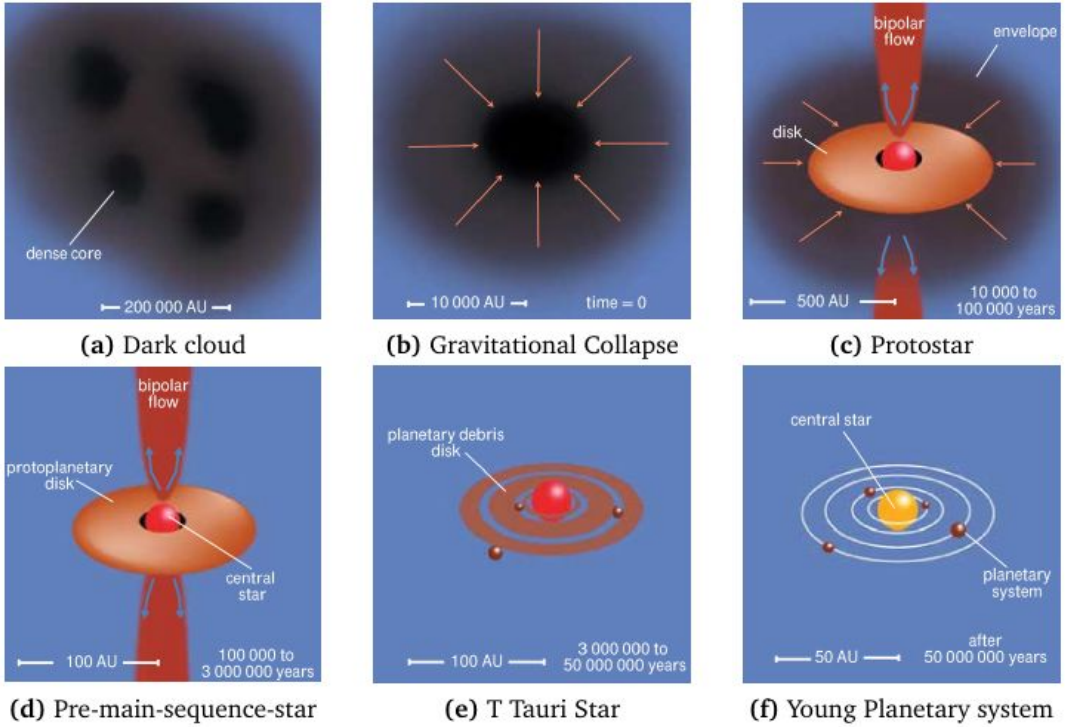

Figure 1: Stages of formation of a Sun-like star. **Credit:** Greene, 2001

A2. Dust properties

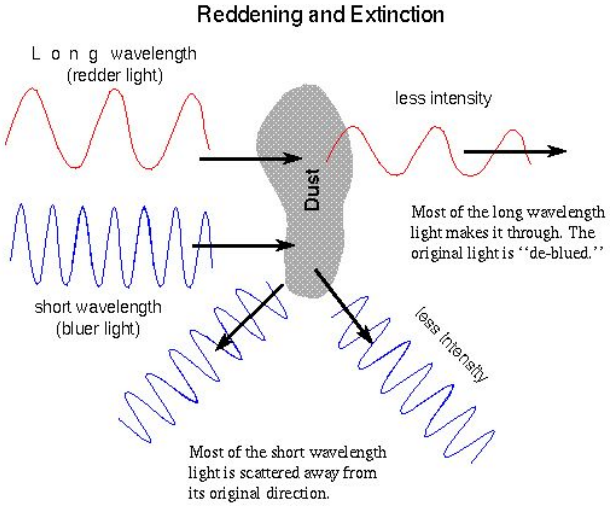

(a) Barnard 68 three-color composite reproduced from one blue (B), one green-yellow (V) and one near-infrared (I) exposure [1]

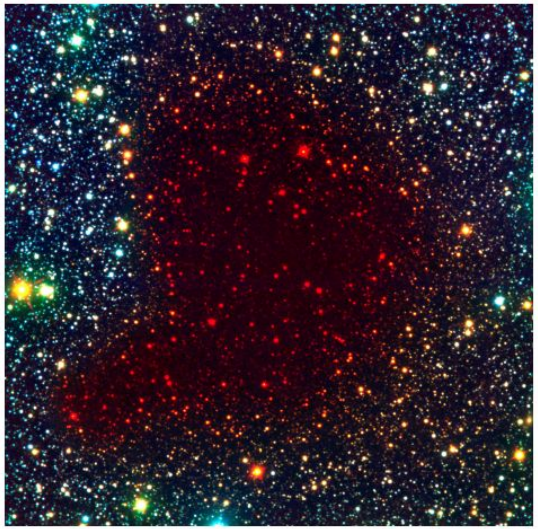

(b) Barnard 68, false-colour composite based on a visible (here rendered as blue), a near-infrared (green) and an infrared (red) image [2]

[1],[2] **Credit:** ESO

A3. Instruments

Name	Number of Telescopes	Diameter [m]	Maximum baseline	λ
Keck I	2	10	85	NIR, MIR
VLTI/MIDI	2/2	8/1.8	130 / 200	MIR
VLTI/PIONIER	4	8/1.8	130 / 200	NIR
VLTI/MATISSE	4	8/1.8	200	NIR, MIR
VLTI/AMBER	3	8/1.8	140	NIR
ALMA	66	12	16 000	radio

A4. T Tauri Data

Star name	Type	distance d[pc]	T_{eff}[K]	L [$L_{\odot}$]	$L_{\text{min}}[L_{\odot}]$	$L_{\text{max}}[L_{\odot}]$
LkHalpha330	T Tauri	250	5800	11	7	16
RYTau	Herbig Ae/Be	142	**6310**	15	9	**23**
LkCa16	T Tauri	142	4350	0.8	0.6	1
DRTau	T Tauri	142	4060	1.1	0.9	1.3
GMAur	T Tauri	142	4730	1.2	0.8	1.6
Tcha	T Tauri	108	5890	1.2	0.5	3.1
HD142560	T Tauri	150	4000	3.7	2.2	5.6
HD143006	T Tauri	145	5884	3.4	2.7	4.2
V2246OPH	T Tauri	120	5248	7.5	6.3	9.5
HBC639	T Tauri	120	5250	8.1	4.8	11.8
ELIAS2-24	T Tauri	120	4266	1.8	1.1	2
ELIAS2-28	T Tauri	120	4169	0.3	**0.2**	0.6
ELIAS2-30	Herbig Ae/Be	120	5950	6.3	3.3	11.9
V2129OPH	T Tauri	120	**3981**	1.3	0.8	1.7
V2062OPH	T Tauri	120	4900	1.5	1	2.1

References

BECKWITH, S. V. W.: Circumstellar Disks. In: LADA, C. J. (Hrsg.) ; KYLAFIS, N. D. (Hrsg.): NATO Advanced Science Institutes (ASI) Series C Bd. 540, 1999 (NATO Advanced Science Institutes (ASI) Series C), S. 579

BRUNNGRÄBER, R.: Beobachtbarkeit von ausgewählten Strukturen und Staubeigenschaften zirkumstellarer Scheiben in verschieden Entwicklungsstadien, Dissertation, CAU Kiel, 2018

COHEN, MARTIN AND EMERSON, J. P. AND BEICHMAN, C. A.: A reexamination of luminosity sources in T Tauri stars. I - Taurus-Auriga. In: Astrophysical Journal 339 (1989), S. 455–473

GREENE, T. P.: Protostars. In: American Scientist 89 (2001), S. 316–325

KARTTUNEN, H. ; KRÖGER, P. ; OJA, H. ; POUTANEN, M. ; DONNER, K. J.: Fundamental Astronomy. 6. Springer, 2017. http://dx.doi.org/https://doi.org/ 10.1007/978-3-662-53045-0. http://dx.doi.org/https://doi.org/10.1007/978-3-662-53045-0. – ISBN 978–3–662–53044–3

LYNDEN-BELL, D. ; PRINGLE, J.E.: The evolution of viscous disks and the origin of the nebular variables. *Monthly Notices of the Royal Astronomical Society,* 168:603-637, 1974

OBER, F.; WOLF, S.; URIBE, A.; KLAHR, H.: Tracing planet-induced structures in circumstellar disks using molecular lines, *Astronomy & Astrophysics*, 601, May 2017

PERCY, J.R.: Understanding Variable Stars, ISBN: 9780521232531, 2007

SHAKURA, N. ; SUNYAEV, R.: Black holes in binary systems. Observational appearance. *Astronomy & Astrophysics,* 24:337-355, 1973